Thermal Effects in the Numerical Simulation of the Thermoforming of Multilayered Polymer Sheets

Michel Bellet, Marie-Hélène Vantal, Bernard Monasse

Int. Polymer Processing 13 (1998) 299-308

Thermal effects in the numerical simulation of the thermoforming of multilayered polymer sheets

Michel Bellet, Marie-Hélène Vantal and Bernard Monasse*

Centre de Mise en Forme des Matériaux, Ecole des Mines de Paris, Sophia Antipolis, France

* Mail address : Dr. B. Monasse, Centre de Mise en Forme des Matériaux, Unité de Recherche Associée au CNRS n°1374, Ecole des Mines de Paris, BP 207, 06904 Sophia-Antipolis Cedex, France

ABSTRACT

This paper mainly treats the thermal effects during the thermoforming process while most of the previous analyses consider an isothermal deformation. A non isothermal three dimensional finite element model of the thermoforming process is proposed. It couples the thermal equations in the thickness and mechanical equations on the mean surface of the sheet. The mechanical resolution is done by a finite element method using a membrane approximation. The deformation is driven by a pressure difference through the sheet. The thermal resolution uses a one dimension finite element method in the thickness with convection or conduction at the surface and dissipation of mechanical energy. The polymer cooling is very efficient during the contact with tools. The coupling is done by the thermal dependent rheology. The respective contribution of friction and thermal effects in the thickness of the part during the process are discussed. The model also considers a possible multilayered material, with specific rheological parameters inside each layer. The rheology of a polystyrene was measured under elongation as a function of temperature, strain and strain-rate and described by a visco-plastic law. The predictions of the model were compared with measurements on an instrumented thermoforming machine and with the local thickness of axisymmetrical parts and with 3-D parts thermoformed with the same polystyrene.

1 INTRODUCTION

The thermoforming process consists of heating a polymer sheet and shaping it inside a mold ([1], see fig.1). The deformation results from an applied differential pressure between the upper and lower side of the sheet, varying with time, and eventually coupled with the use of a moving plug. The forming of thin products made of various polymer materials is carried out by this method : rubbery amorphous, solid semi-crystalline or multi-layer composites. The heating temperature depends upon the selected polymer. At low temperature, the forming is limited by the high rigidity of the sheet. On the contrary, at high temperature, the sheet deforms by gravity and the forming is very difficult to control. Hence, thermoforming is performed above the glass transition temperature (T_g), in the rubber-like behavior domain, for amorphous polymers, and close to the melting temperature for semi-crystalline polymers.

One of the main problems of the process is the thinning in the corners of the parts, which leads to a decrease of the mechanical properties of the shaped components. The optimization of the final thickness profile is generally achieved by trial-and-error, changing the design of the component, the polymer material, and the process parameters such as the heating temperature distribution, the mold temperature, the pressure curve, or using a plug for deep parts. The numerical modeling of the shaping stage should then result in a more efficient optimization of the process : this is the point on which the present paper is focused.

Various numerical simulation models have been proposed [2-7]. Concerning the application to three-dimensional forming, they are generally based on the membrane mechanical approximation, associated with the finite element method. Those computations use either hyperelastic [3, 5-7] or viscoelastic [2, 4] constitutive equations, without any heat transfer coupling, and a sticking contact hypothesis at the polymer-tool interfaces. It should be pointed out that this latter assumption has no experimental support. Most of the time, it is used just because the computation is isothermal and cannot account for the decrease of the polymer temperature and its "freezing" after tool contact. These models are unable to predict the effect of the mold temperature. Another thermo-mechanical coupling is the self heating source term due to the high strain rates**.** As the thermal diffusivity is low and the behavior highly temperature dependent, it seems essential to couple the heat transfer and mechanical models.

In the present paper, on-line measurements on a thermoforming machine are done and compared with the kinematics predicted by the three dimensional finite element code. Local thickness measurements on the final product check another prediction of the thermo-mechanical model. Concerning the contact conditions with plug and mold, either sliding contact with Coulomb's friction law or sticking contact can be considered. The paper is focused on the thermal evolution effects during the forming, and on its role in the process compared to mechanical effects such as contact conditions. Then a first approach to multilayered sheet forming is proposed.

2 MATERIAL AND EXPERIMENTAL METHODS

2.1 Thermoforming device

The experiments were done on two different Kiefel thermoforming machines : an instrumented machine with an axi-symmetrical mold, and an industrial in-line machine including multi-imprints with non symmetrical shapes.

On the industrial Kiefel machine the infra-red heating and thermoforming sequence is fixed. The forming is driven by pressure without any operating plug. This industrial machine is not instrumented, the maximum pressure applied is known (P = 0.6 MPa) but not the pressure variation during the forming process. Thus it is not possible to check the kinematics of the film during the process. It is only possible to measure the final profile along various directions of a complex geometry. With this device the robustness of the three dimensional finite element code and its ability to predict a complex shape can be tested. A polypropylene is thermoformed in this machine and the rheology under uniaxial tension was measured previously [8].

The pilot machine Kiefel KD20/25 includes two positions : a heating zone and a forming position. The different steps of the sequence heating - transfer - forming are controlled separately. The heating of the film is done by two plates including twelve quartz infra-red heaters each. The thermal homogeneity of the film is controlled by the individual adjustment of the power of the heaters. The temperature is measured in the center of the film by an infra-red sensor up to the final temperature, then the film is automatically transferred to the forming zone. The forming can be done by a differential pressure with pressure on the top and air

pumping in the mold (Fig. 2). The aluminum mold can be heated. It is composed of two parts : a basically truncated conical cavity and an axial removable insert. The mold geometry is mainly characterized by the depth/radius ratio d/r = 60 mm / 70 mm to produce a significant deformation of the film. The insert must anticipate the film contact and then the contact contribution on further deformation. The mold is instrumented with pressure, temperature and contact gauges in various locations of the mold. The temperature is measured on the film with an infra-red sensor fixed on the mold just after the transfer from heating zone to take into account possible cooling. This temperature is the initial thermal condition for the forming process. The pressure is measured on the top of the cover and in the outer corner of the mold (Fig. 2). The contact of the polymer with the mold is detected by four sensors located in critical regions including the first contact, on the insert, and the last ones, in the corners of the mold. The pressure sensors were calibrated in static condition at P = 0.1 MPa and a maximum error of $\delta P = 5\ 10^{-4}$ MPa was measured on each sensor. Then it is possible to measure precisely ($\delta P = 10^{-3}$ MPa) the pressure difference through the sheet during the thermoforming process.

Figure 3 presents a typical measurement of pressures in the cover P_o and in the mold P_1, respectively, and the contact time of the various contact gauges (C1, C2, C3). The differential pressure ΔP which acts on the deformation of the film is deduced from pressure measurements, $\Delta P = P_o - P_1$ (Fig. 3). The measured differential pressure ΔP or cover pressure P_o will be applied in the thermo-mechanical model. The time contact measured and predicted by the model will be compared.

The forming parameters are as follows:

T_m = 20°C or 60°C for the mold,

T_{air} = 20°C,

$d(P_o)/dt$ = 0.125 ; 0.36 or 0.6 MPa.s^{-1} up to 0.1, 0.2 or 0.4 MPa, respectively,

$\Delta P = f(t)$ are deduced from on-line measurements,

T_s = 110, 130 or 140°C for the sheet.

2.2 Polymer and elongational rheology

An atactic polystyrene provided by the ELF-ATOCHEM Company was mainly used during these experiments. It is a blend of 50% impact polystyrene with 50% crystal

polystyrene, $\overline{M}_w$ = 1.9 10^6 g/mol ($\overline{M}_w / \overline{M}_n$ = 3) and $\overline{M}_w$ = 2.2 10^6 g/mol ($\overline{M}_w / \overline{M}_n$ = 2.6) respectively. The polymer was provided as extruded polymer sheets 0.3 mm thick and 20 cm large.

The rheology under uniaxial elongation of polystyrene is measured using a sheet in an isothermal condition under a constant strain rate $\dot{\varepsilon}$. The experiments were done with a hydraulic tensile machine, Instron 1341, in an oven with a transparent door to observe the sample as it is heated by convected air. A sample 20 cm long and 15 cm wide is cut in an extruded cast-film with respect to the processing conditions. It is marked with a regular grid ΔL_o = 1 mm and Δl_o = 5 cm, respectively along the length and the width directions. Its distortion during the experiment gives the local Hencky deformation $\varepsilon = \ln(\Delta L / \Delta L_o)$. The sample is clamped around cylindrical jaws to reduce the gauge-length to 3 cm. The tensile machine is piloted with an exponential head displacement up to L_{max} = 15 cm to fix a constant strain rate $\dot{\varepsilon}$. Photographs are shot during experiments to measure the deformation, and to detect a possible heterogeneity of deformation.

The experiments are done on the polystyrene at four temperatures (110°C, 120°C, 130°C, 140°C) and four strain-rates for each temperature in the range 10^{-4} s^{-1} $\leq \dot{\varepsilon} \leq$ 10^{-2} s^{-1}. The temperature range was chosen to provide measurements in the rubber state above $T_g \approx$ 90°C. The deformation is not really homogeneous and an analysis of the local deformation was applied to measure the true stress as a function of true strain (Fig. 4). The rheology markedely changes with temperature. The stress and the strain hardening effect under large deformation strongly decrease with temperature. The strain rate sensitivity of the stress increases with temperature. This complex rheology can be represented by a one-dimensional constitutive equation initially proposed by G'Sell and Jonas [9]. It has been selected in the context of polymer thermoforming:

$$\bar{\sigma} = K_p(T)\left[1 - \exp(-w\bar{\varepsilon})\right] \exp\left(h\bar{\varepsilon}^2\right) \dot{\bar{\varepsilon}}^m \qquad (1)$$

where T is the temperature, $\dot{\bar{\varepsilon}}$ the von Mises equivalent strain-rate, $\bar{\varepsilon}$ the von Mises equivalent strain, and K_p, w, h and m are, respectively, the consistency, the viscoelastic strain hardening and strain rate coefficients of the polymer. These results are completed by data

from literature [10, 11] (Fig. 5). The consistency K_p of the material decreases suddenly above T_g and keeps low values (≈2 MPa.s^m) in the experimental domain. The so-called viscoelastic coefficient w is found to be low (≈3.7) and independent on temperature. The low temperature behavior is characteristic of a solid-like material, i.e., with a significant strain-hardening and a low strain-rate exponent (Fig. 5). At high temperature the polymer is a fluid-like material, i.e., no strain-hardening and a large strain-rate coefficient. Consequently, the rheology changes in the temperature range 110°C - 140°C, well above the glass transition.

This rheological model is able to describe the mechanical behavior of a great number of polymers, either amorphous or semi-crystalline, for a large temperature range. The parameters for polypropylene have been identified for a large temperature range (20°C ≤ T ≤ 150°C) by means of tensile tests on sheets with the same range of deformation rate [9] :

$$K_p = 5.31\ 10^{-3} \exp [2.85\ 10^{-3} / T] \text{ MPa.s}^m \qquad w = 30,\ h = 0.4,\ m = 0.04$$

For polypropylene only the consistency K_p significantly depends on temperature, the value of the other parameters remain almost constant. These rheologies, model and parameters, are included in the finite element code to predict the polymer deformation coupled with thermal effects.

3 3-D THERMO-MECHANICAL MODEL FOR A MULTILAYERED MATERIAL

3.1 Mechanical model and resolution

In this section, we will present briefly the mechanical approach used in the finite element model Tform 3, in which the previous constitutive equation has been implemented. The reader can refer to [12-13] for a more detailed description of the mechanical model and its numerical discretization. According to the membrane assumption, the deformed sheet is considered as a geometric surface, neglecting flexure and transverse shear. A material point is identified by two curvilinear coordinates: $\theta 1$ and $\theta 2$ which are, in the case of an initial sheet in the xy plane, of the initial x and y coordinate respectively. Hence, at any point M on the deformed sheet (vector **x**) the local tangent basis is defined by:

$$\mathbf{g}_1 = \frac{\check{Z}\mathbf{x}}{\check{Z}\theta^1} \qquad \mathbf{g}_2 = \frac{\check{Z}\mathbf{x}}{\check{Z}\theta^2} \qquad \mathbf{g}_3 = \frac{1}{\|\mathbf{g}_1 x \mathbf{g}_2\|}\, \mathbf{g}_1 x \mathbf{g}_2 \tag{2}$$

where x denotes the vectorial product. The equilibrium of the deformed sheet is expressed by the principle of virtual work (without inertia effects):

$$\forall \mathbf{v}^* \int_\Omega \boldsymbol{\sigma}^{ij} v^*_{i|j} e dS - \int_{\Omega_p} P\mathbf{g}_3.\mathbf{v}^* dS - \int_{\Omega_c} \mathbf{t}.\mathbf{v}^* dS = \mathbf{0} \tag{3}$$

in which Einstein's convention of summation of repeated indices is used, as in the sequel. σ_{ij} are the covariant components of the Cauchy stress tensor (plane stress: i,j = 1,2), $.|_j$ denotes covariant derivation with respect to the θ_j material coordinate. In the first term, the virtual power dissipated by the normal and shear stresses are neglected compared to the virtual power dissipated by the normal and shear stresses is neglected compared the virtual power dissipated by in-plane stresses due to the sheet expansion. Then the summation is extended only to i,j=1,2. Practically, a plane stress assumption is used, with only three components in the symmetric stress tensor. The variable e is the sheet thickness, **t** are the friction stresses on regions Ω_c on the sheet contacting the mold, P is the inflation differential pressure applied to the domain Ω_p of the deformed surface Ω.

Starting with a balanced configuration Ω at time t, the problem consists of determining the unknown equilibrated configuration Ω' at $t+\Delta t$. Variables at $t+\Delta t$ are denoted by "prime". For application of eq. (3) at $t+\Delta t$, we have, for any velocity field **v***:

$$\int_{\Omega'} \boldsymbol{\sigma}'^{ij} \mathbf{v}^*_{i|j}\, e' dS - \int_{\Omega'_p} P'\mathbf{g}'_3.\mathbf{v}^* dS - \int_{\Omega'_c} \mathbf{t}'.\mathbf{v}^* dS = \mathbf{0} \tag{4}$$

This equation is solved for the incremental displacement field **u** between Ω and Ω', provided that **t'**, e' and **σ'** can be calculated from **u**. Those relations are exposed hereunder with the resolution of (4).

- Contact and friction : the contact condition applied to Ω_c may be either sticking (no relative velocity with respect to the mold) or sliding. In this case, the tangential stress is given by Coulomb's friction law (coefficient μ), in which the normal stress is the inflation pressure:

$$\mathbf{t'} = -\mu P' \, (1 / ||\mathbf{u}||) \, \mathbf{u}\,\mathbf{t} \qquad (5)$$

- Thickness updating: the new local thickness e' is deduced from material incompressibility. Denoting **g** the metric tensor ($g_{ij} = \mathbf{g_i}.\mathbf{g_j}$), we have the following relation (6), which permits, for a given displacement field **u** to evaluate **g'** and so update the thickness e' :

$$e' = e \sqrt{\det(\mathbf{g}) / \det(\mathbf{g'})} \qquad (6)$$

- Resolution of incremental constitutive equations : the one-dimensional constitutive equation (1) can be written as a classical viscoplastic power law:

$$\bar{\sigma} = k \, \bar{\varepsilon}^{m} \qquad (7)$$

in which the k is the so-called viscoplastic consistency. Hence, the flow rule derives from a viscoplastic potential Q. Under the assumption of isotropy, it yields :

$$\dot{\boldsymbol{\varepsilon}} = \frac{\check{Z}Q}{\check{Z}\boldsymbol{\sigma}} = \frac{\check{Z}Q}{\check{Z}\bar{\sigma}} \frac{\check{Z}\bar{\sigma}}{\check{Z}\boldsymbol{\sigma}} = \dot{\bar{\varepsilon}} \frac{\check{Z}\bar{\sigma}}{\check{Z}\boldsymbol{\sigma}} \qquad (8)$$

In convective curvilinear coordinates, the equivalent von Mises strain rate $\dot{\bar{\varepsilon}}$ is expressed as :

$$\dot{\bar{\varepsilon}}^2 = 2/3 \, \dot{\varepsilon}^{ij} \dot{\varepsilon}_{ij} \qquad (9)$$

in which $\dot{\varepsilon}^{ij}$ and $\dot{\varepsilon}_{ij}$ denote the covariant and contravariant components of the strain rate tensor $\dot{\boldsymbol{\varepsilon}}$, respectively.

The equivalent von Mises stress has a similar expression, with the covariant and contravariant components of the deviatoric stress tensor **s** :

$$\bar{\sigma} = \sqrt{\frac{3}{2} s^{ij} s_{ij}} \qquad \mathbf{s} = \boldsymbol{\sigma} + p\mathbf{I} \qquad s^{ij} = \sigma^{ij} + p \, g^{ij} \qquad (10)$$

Taking into account the above plane stress assumption, the hydrostatic pressure p is given by :

$$p = -\frac{1}{3} \mathrm{Trace}(\sigma) = -\frac{1}{3} \sigma^{ij} g_{ij} \qquad i, j = 1,2 \qquad (11)$$

and the equivalent von Mises stress can be written :

$$\bar{\sigma} = \sqrt{\sigma^{ij} A_{ijkl} \sigma^{kl}} \qquad (12)$$

with

$$A_{ijkl} = \frac{3}{2} g_{ik}g_{jl} - \frac{1}{2} g_{ij}g_{kl} \qquad i,j,k,l = 1,2 \tag{13}$$

Using now the vectorial notation $\underline{\sigma} = \left[\sigma^{11}\ \sigma^{22}\ \sigma^{12}\right]^T$, we have :

$$\bar{\sigma}^2 = \underline{\sigma}^T \underline{\mathbf{A}}\ \underline{\sigma} \tag{14}$$

where $\underline{\mathbf{A}}$ is a symmetric 3x3 matrix defined by :

$$\underline{A}_{11}=A_{1111}\ \ \underline{A}_{22}=A_{2222}\ \ \underline{A}_{33}=A_{1212}\ \ \underline{A}_{12}=A_{1122}\ \ \underline{A}_{13}=A_{1112}\ \ \underline{A}_{23}=A_{2212} \tag{15}$$

The constitutive equation can then be written:

$$\dot{\underline{\varepsilon}} = \frac{\dot{\bar{\varepsilon}}}{\bar{\sigma}} \underline{\mathbf{A}}\ \underline{\sigma} = \frac{1}{k} \dot{\bar{\varepsilon}}^{(1-m)} \underline{\mathbf{A}}\ \underline{\sigma} \tag{16}$$

where $\dot{\underline{\varepsilon}} = \left[\dot{\varepsilon}_{11}\ \dot{\varepsilon}_{22}\ \dot{\varepsilon}_{12}\right]^T$. A semi-implicit time integration scheme is used over the increment. The incremental strain tensor $\Delta\varepsilon$, the covariant components of which depend on the displacement **u** according to (17) are written as (18):

$$\Delta\varepsilon_{ij} = 1/2\ (u_{i|j} + u_{j|i} + u_{m|i}u^m_{|j}) \tag{17}$$

$$\Delta\underline{\boldsymbol{\varepsilon}} = \Delta t \left[(1-\eta)\ \dot{\underline{\boldsymbol{\varepsilon}}} + \eta\ \dot{\underline{\boldsymbol{\varepsilon}}}'\right] \tag{18}$$

Equations (16-18) clearly permit determination of the new local stress tensor σ', knowing the displacement field **u**. A fully implicit scheme (η=1) is used (Euler backward scheme).

Finally, substitution of (5-6) and (16-18) in the equilibrium equation (4) leads to a non-linear equation for the displacement field **u**. Its spatial discretization by the standard Galerkin finite element method (linear triangles or quadrangles) is detailed by Bellet [12, 13]. Let us denote [**N**] the interpolation matrix and [**B**] the differentiation matrix defined by :

$$\mathbf{u} = [\mathbf{N}]\ \mathbf{U} \qquad\qquad \underline{\boldsymbol{\varepsilon}} = [\mathbf{B}]\ \mathbf{V} \tag{19}$$

The discretized form of the equilibrium equation can be written as :

$$\mathbf{R}(\mathbf{U}) = \int_{\Omega'} [\mathbf{B}']^T \underline{\sigma}' \, e' \, dS - \int_{\Omega'_p} P' \, [\mathbf{N}]^T \, g'_3 \, dS - \int_{\Omega'_c} [\mathbf{N}]^T \, t' \, dS = 0 \qquad (20)$$

Hence, at every time step a non-linear system for the vector **U** of the nodal displacements is solved by the Newton-Raphson method. It should be noted that a consistent tangent matrix $\partial\mathbf{R}/\partial\mathbf{U}$ can be expressed.

Regarding contact treatment, the simulation code can handle several tools (punch or molds) that are supposed to be rigid. Their surfaces are discretized in triangular elements, so that it is possible to evaluate the relative positions of the nodes of the finite element mesh of the sheet, at each time increment. In case of slight penetration of a node in the tool, the normal displacement of this node comes back to the tangential tool surface. In addition, to prevent such undesirable effects, the nodes that are found in a thin boundary layer at the neighborhood of the tool surface are considered to be in contact and their normal displacement to the tool is prescribed equal to zero.

3.2 Thermal model and coupling

Considering the thinness of polymer sheets, the short processing times, and the low thermal diffusivity of polymers, it can be assumed that heat transfer is essentially one dimensional across the thickness of the sheet [14]. Consequently, s being the coordinate in the thickness direction ($s=\theta_3$), the 1D heat transfer equation can be expressed:

$$\rho c \frac{dT}{dt} = \frac{\partial}{\partial s}\left(\lambda \frac{\partial T}{\partial s}\right) + \boldsymbol{\sigma} : \dot{\boldsymbol{\varepsilon}} \qquad (21)$$

where ρ is the specific mass, c the heat capacity and λ the heat conductivity. The following boundary conditions are accounted for. At sheet/air interface:

$$-\lambda \frac{\partial T}{\partial s} \mathrm{sgn}(\mathbf{n}) = h_{conv} \, (T - T_{air}) \qquad (22)$$

where h_{conv} is the coefficient for heat exchange by convection, T_{air} the air temperature and sgn(**n**) is ±1 depending on the orientation of the outward normal unit vector **n**. At sheet/tool interface the surface temperature of the polymer sheet is prescribed by the interface temperature :

$$T_{inter} = (b_m T_m + b_s \bar{T}_s) / (b_m + b_s) \quad (23)$$

where b is the thermal effusivity $\sqrt{\lambda \rho c}$ and $\overline{T}_s$ is the average temperature in the thickness of the sheet. The initial temperature profile is assumed to be known at the beginning of the process. The following values of the thermal parameters characterize polystyrene: $\rho c = 1.92\ 10^6$ J.m^{-3}.K^{-1}, $\lambda = 0.2$ W.m^{-1}K^{-1}, h = 33 W.m^{-2}.K^{-1}. Coulomb friction has been accounted for ($\mu = 0.4$) [15, 16].

Equation (14) is discretized in space and time, at each integration point of membrane, using a Galerkin 1D finite element method with linear three node elements (Fig. 6) and a semi-implicit Crank-Nicholson time integration scheme [14]. The coupling between the mechanical and the thermal solution is carried out at each time increment as explained in figure 7.

3.3 Multilayer formulation

The multilayer approach proposed here is based on the following assumptions:

- each layer is subjected to the same deformation as the mean surface of the sheet. This is consistent with the membrane approach and the thickness ratio of the different layers remains constant during the process.
- accordingly, the mechanical and thermal contacts are assumed perfect (no sliding, no thermal contact resistance) at interfaces between layers.

The algorithm is identical to the one for heat transfer coupling, except that all thermal and mechanical parameters used at integration points in thickness (ip_th) will now depend upon the material in which they are located (Fig. 8). Each material layer has an identified temperature dependent material law. A mean stress is then calculated from each stress contribution inside the thickness. Such a formulation is expected to be more precise than the reduction of the multilayer to a single "equivalent" material, especially when steep temperature gradients appear in the sheet thickness when one side of the multilayer contacts the tooling.

4 RESULTS

4.1 Axisymmetric thermoforming test

For the axisymmetric mold, only a 11°25' sector has been meshed with 160 triangles.

4.1.1 Thermal effect in the thickness of the sheet during the forming process

The initial orientation of the polystyrene sheet due to extrusion is relatively high, and it involves an evolution of the thickness during infrared heating as it is clamped. Consequently, the measured final thickness profile depends upon the measurement direction (extrusion or transverse direction, Fig. 9). The measurements shall be done along the extrusion direction to be consistent with the measured rheology.

The thermal effects shall be first considered. It is possible to predict the thermal gradient across the thickness of the sheet during the whole process (Fig. 10) and in the deeper part of the mold (Fig. 11). During the stretching in air the thermo-mechanical model predicts a very low heating due to the deformation in the sheet and a very low cooling due to air convection at the surface. The deformation is nearly isothermal (temperature variation less than 10°C). During this period the thickness of the sheet decreases (Fig. 10, 11). The polymer is quickly cooled after the contact with the mold and a large thermal gradient appears. A gradient of stress develops inside the thickness of the sheet as the result of the thermal dependence of the rheology. The contact on the insert is reached near the beginning of the forming process. The long heat transfer time inside the thick part allows a sliding of the sheet from 0.1s to 0.25s resulting in a continuation of the thinning of the film. After this period the cooling effect on the rheology is sufficient to balance in the plane stress and nearly halt the deformation (Fig. 10). On the contrary, the cooling of thinner film (higher deformation at the contact time) fixes almost instantaneously the polymer to the mold. The in plane stress is not sufficient to counterbalance thermal effects in the film. This mean the stress quickly increases in that position of the mean surface of the sheet. The deformation is nearly stopped in that position as an effect of the equilibrium relationship on the sheet (eq. 3). Consequently the thickness of the sheet in that position is nearly fixed by the cooling (Figs. 10 and 11). This thermal effect coupled with a moderate but realistic friction coefficient ($\mu = 0.4$) leads to a very efficient freezing of the polymer during contact with a low temperature mold (Fig. 12). The result is not so different from the sticking condition usually considered in most of the isothermal models. Sticking has no physical sense, since independent measurements always give a very low value for the friction coefficient of a solid polymer on a metal [15, 16]. The present non-

isothermal formulation clearly uncouples the frictional and the thermal effects. If sticking is nevertheless considered there is no effect of the nature or temperature of the mold on the thickness profile and no possible processing action except the temperature control of the sheet. If the boundary condition is mainly dominated by the mold temperature this parameter can be used to favor a limited sliding to produce a more homogeneously thick part.

4.1.2 Prediction of processing time

The deformation of the sheet was simulated in various pressure histories and various temperatures for the polymer and the mold. The simulated time contact and measured values are systematically compared. When the differential pressure ΔP measured by the gauges is applied in the model the time of contact is always overestimated by a large factor, more than five. For example with the condition described in figure 10 the sheet is in contact at 0.095 s with the central insert when the model predicts more than 0.48 s to reach this position. The discrepancy between measurements and predictions is not explained. It must be noticed that the location of these pressure gauges give static pressure and should underestimate the pressure applied on the sheet.

Further calculations consider only the upper pressure P_o. The predictions of time contact fit accurately the measurements for the various applied thermal and pressure conditions (Fig. 13). It is possible to analyze the effect of processing parameters on the time of contact either using the direct measurements or the predictions of the model. The upper pressure increases almost linearly with time up to the maximum pressure (Fig. 3). The measurements and the model show that the polymer is thermoformed during the transient period (Figs. 3 and 13). The pressure rate shall be considered as the representative mechanical parameter and not the maximum pressure. It is the main mechanical parameter acting on the kinematics and hence on the time of contact (Fig. 14). An increase in the temperature of the polymer slightly decreases the time of contact (Fig. 14). This decrease is surprisingly low when the rheology shows a strong change of mechanical behavior in this temperature range (110 - 130°C) (Figs. 4 and 5). A higher polymer temperature leads to a higher strain rate coefficient (Fig. 5). During the forming process the strain rate effect partly counterbalances the thermal effect on the consistency K_p. These are the two main rheological parameters acting on the polymer deformation. The strain hardening coefficient h has a small effect in this range of deformation and is slightly more prominant near the end of the forming process. The mold temperature, up

to T_m = 60°C, does not significantly affects the time of contact, the slight change of the boundary condition induced by the cooling of the sheet in contact with the mold has a tiny effect on the remaining free part of the sheet.

4.1.3 Prediction of the final thickness

The thickness variation is calculated for each position throughout the thermoforming process. The local thickness can be shown along the radius of the part, more precisely on the projection along the radius. The mould geometry with a central insert is considered. The predicted and measured final thickness can be compared. The final thickness is calculated with various thermal (thermal or isothermal) and boundary (sticking or friction) conditions. The thickness predicted by all the models is almost the same over most of the geometry. They differ significantly only at the contact with the insert. As it can be seen from figures 9 to 12, the isothermal model with friction ($\mu = 0.4$) predicts an unrealistic thinning of the polymer on the insert ($x \leq 20$ mm). This thinning comes from the sliding of the polymer sheet on the insert. The polymer rheology under isothermal condition is unable to halt the deformation. On the contrary a very large thickness is predicted on the insert when a sticking condition is applied with either an isothermal or non isothermal model. The thermal model is necessary to predict the thickness with areasonable value of the friction coefficient ($\mu = 0.4$). It appears that thermal effects are very efficient at halting the polymer deformation. The deformation is then located in zones where the temperature is still higher, i.e., without any previous contact with the mold. In these thermal conditions, cooling has almost the same effect as the boundary conditions. The non-isothermal model is much more representative of the local phenomena in thermoforming. It is able to account independently for interface tribology and heat transfer, and finally results in a very good agreement between measured and computed thickness profiles.

4.1.4 Orientation in polystyrene part

Model and experiments predict the same heterogeneous deformation. The thinning, mostly located in the corners, results from an elongation which can induce an orientation of the polymer. This orientation acts to increase the mechanical properties. It can partly

counterbalance the local thinning of the industrial part. The size and geometry of the part lead to difficult measurements of the local mechanical properties. The local polymer orientation , measured by birefringence, was used to check the possible heterogeneity of the mechanical properties. A K compensator on a Reichert Zetopan-pol microscope was used to measure the optical path difference $\Delta\lambda$. The birefringence is deduced from the local thickness knowledge e, $\Delta n = \Delta\lambda / e$. These birefringence measurements were done along the radius for two processing conditions (Fig. 15). The strong condition (high pressure P = 0.4 Mpa, T_S = 130°C) minimizes the relaxation of polymer chains and leads to a higher orientation than the soft condition (low pressure P = 0.1 Mpa, T_S = 140°C). Both conditions produce the highest orientation in the inner corner of the insert (contact sensor C_4 on figure 2) and the lowest at the first contact with the insert (contact sensor C_1). The very low orientaion on the insert results from the very low deformation necessary to reach the contact.No significant sliding appears during the contact of the polymer on this part of the mould. Consequently, no processing effectcan be found in this part of the polymer. On the contrary, the highest deformation (contact sensor C_4) is the most sensitive to processing parameters. The strong conditions must induce the higher orientation and thus the higher mechanical properties.

4.1.4 Multilayer application

We have simulated the forming of a bilayered sheet : 80% polystyrene (PS), 20% polypropylene (PP), total thickness 1 mm. The rheological parameters for both polymers are those given in section 2. The sheet is formed successively with a plug with a 50 mm radius (maximum ram displacement Δz=-30 mm at 0.15 s) and pressure (linear increase of 0.8 MPa between 0.15 s and 0.65 s). The initial temperatures are 20°C for tools and 150°C for the sheet.

The generic shape of the thickness distribution along the radius is due to the punch assisted forming. It is shown in table 1 and Figure 16 that the deformation of the bi-layer is not a simple addition or average of the deformation of each layer component with the same thickness. In addition, the results clearly depend on which material is on top. This is due to the fact that the cooling effect is different for polystyrene or polypropylene : the consistency of polystyrene decreases suddenly above T_g whereas it follows an Arrhenius law for

polypropylene. Also m and h are temperature dependent for polystyrene but constant for polypropylene. This point is to be confirmed experimentally.

4.2 Non axisymmetrical model

In order to test the robustness and the results of the code, the forming of a one-layer shallow component for food packaging has been studied (Fig. 17). Only a quarter of the symmetric industrial forming mold has been computed, using 7591 and 6463 triangles for the sheet and mold meshes respectively. The material is polypropylene, initially 0.475 mm thick. The following parameters can be considered realistic for industrial forming conditions : aluminum mold (5°C), linear pressure reaching 0.7 MPa at 0.5s, air temperature 20°C, initial sheet temperature 150°C. As shown on Fig. 18, the central bulging of the sheet is very fast, reaching the bottom at 0.04s. The forming is then slowed down until the end. Figure 19 shows the deformed finite element mesh at the end of the process. Iso-values of temperature (not shown here) indicate that during forming the free regions are the warmer (close to the initial temperature), and that in contacting regions, the longer the contact duration, the cooler is the sheet. The final thickness of actual parts has been measured along the five directions mentioned on Figure 19. An example of the comparison with the computed values is shown in Figure 20. Experimental points are issued from measurements on two different parts, yielding four values per point. The experimental dispersion has been found high (up to 18% of the average value). The average of the relative errors between computed and average experimental thickness is reasonable : 10% at the bottom, 18% at the wall.

5 CONCLUSION

A thermo-mechanical model including thermal evolution during the process is necessary to predict the deformation, and the final thickness of thermoformed parts. The thermal effect during contact with the tools mainly controls the sliding of the material on the mold. The model includes a temperature dependent visco-plastic rheology whose parameters are measured for a polystyrene under uniaxial elongation with constant strain-rate and isothermal conditions. The polystyrene exhibits a rheological change from liquid to solid like behaviour over a wide temperature range.

9 ACKNOWLEDGMENT

The experimental part of this work has been done at Elf-Atochem (Cerdato) which has also supported this study. In the Elf-Atochem company, Daniel Lebouvier, Jean Claude Jammet and Ronan Andro must be thanked for their support, Stéphane Galliot for the instrumentation and his help for on-line measurements. Prof. J.M. Haudin is thanked for helpful discussions on this paper.

10 REFERENCES

1 *Throne J.L.:* Thermoforming. Hanser Publishers, New-York (1987)

2 *Warby M.K. Whiteman J.R.:* Comput. Struct. 68, p.33 (1988)

3 *De Lorenzi H.G., Nied H.F.:* Modeling of Polymer Processing. A.I.Isayev Ed., Hanser Verlag, 5, p.118 (1991)

4 *Kouba K., Bartos O., Vlachopoulos J.:* Polym. Eng. Sci. 32, p. 699 (1992)

5 *Shrivastava S. Tang J.:* J. Strain Anal. 28, p. 21 (1993)

6 *Allard R., Charrier J.M., Ghosh A., Marangou M., Ryan M.E., Shrivastava S., Wu R. :* 1st Annual Meeting of Polym. Proc. Soc., Akron (1984)

7 *D'Oria F., Bourgin P., Coincenot L.:* Advances in Polym. Technol. 14 (4), p. 291 (1995)

8 *Duffo P., Monasse B., Haudin J.M., G'Sell C., Dahoun A.:* J. Mater. Sci. 30, p.701 (1994)

9 *G'Sell C., Jonas J.J. :* J. Mat. Sci. 14, p. 583 (1979)

10 *Kambour R.P., Robertson R.E. :* Polymer Science, Vol I, ed. Jenkins, University of Sussex, p. 688 (1972)

11 *Mc Crum N.G., Read B.E., Williams G.:* Anelastic and dielectric effects in polymeric solids. John Wiley & Sons, London (1967)

12 *Bellet M.:* Modélisation numérique du formage superplastique de tôles. Doctorate thesis, Ecole des Mines de Paris (1988)

13 *Bellet M., Massoni E., Chenot J.L.:* Eng. Comp. 7, p. 21 (1990)

14 *Vantal M.H.:* Etude numérique et expérimentale du thermoformage des polymères. Doctorate thesis, Ecole des Mines de Paris (1995)

15 *BowdenF.P., Tabor D.*, The friction and lubrication of solids Part II, Clarendon Press, Oxford (1964)

16 *Hironaka s., Komoto T., Tanaka K.*, Wear, 87, p. 85 (1983)

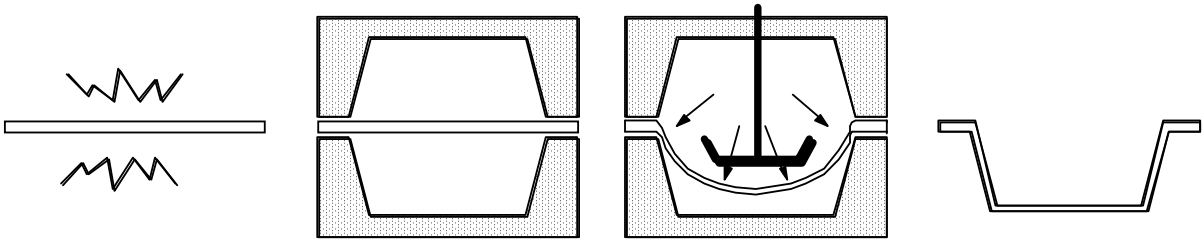

(a) heating (b) shaping (c) cooling

Figure 1 : The different phases of the thermoforming process.

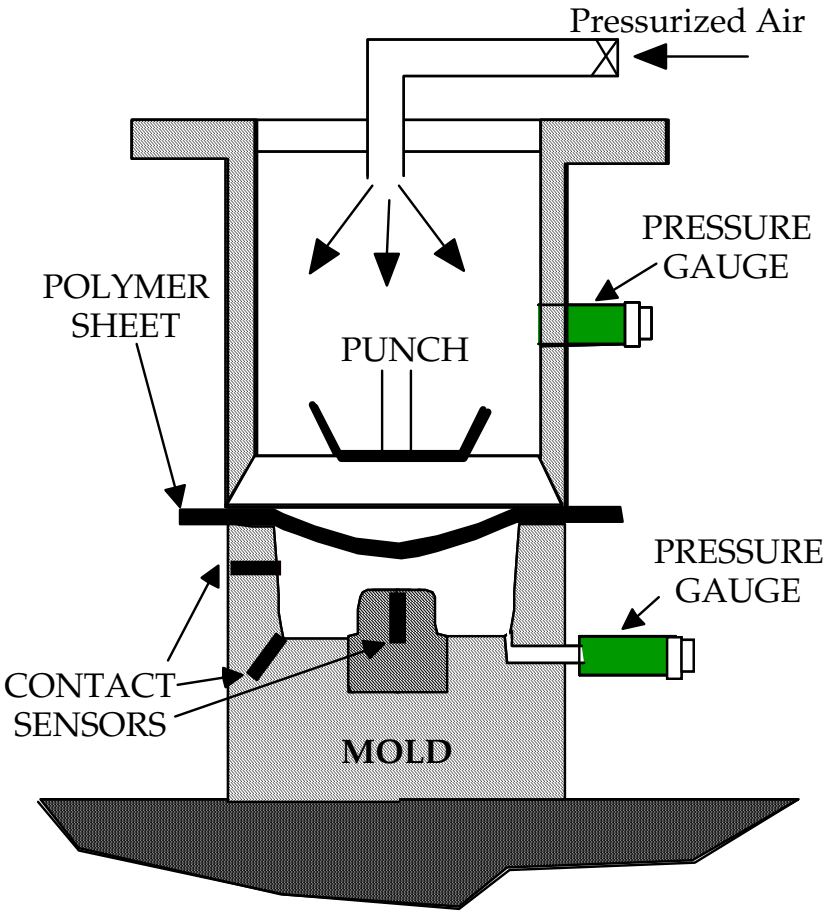

Figure 2 : Axisymmetrical thermoforming machine with contact and pressure sensors.

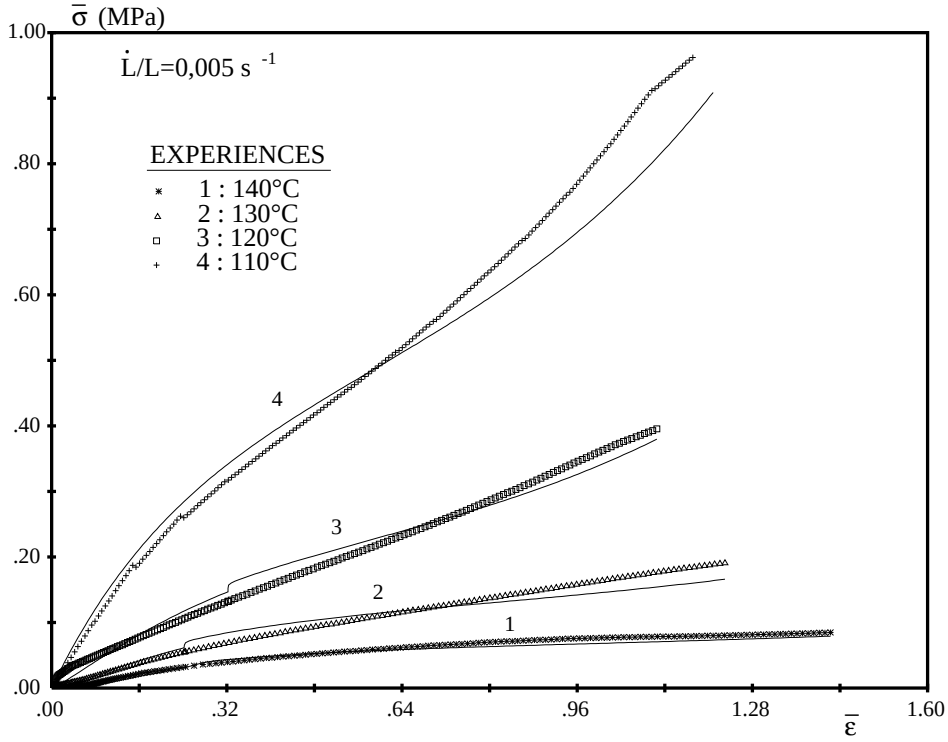

Figure 4 : Uniaxial stress-strain curves measured under constant strain rate ($5\ 10^{-3}\ s^{-1}$) in isothermal conditions for four temperatures.

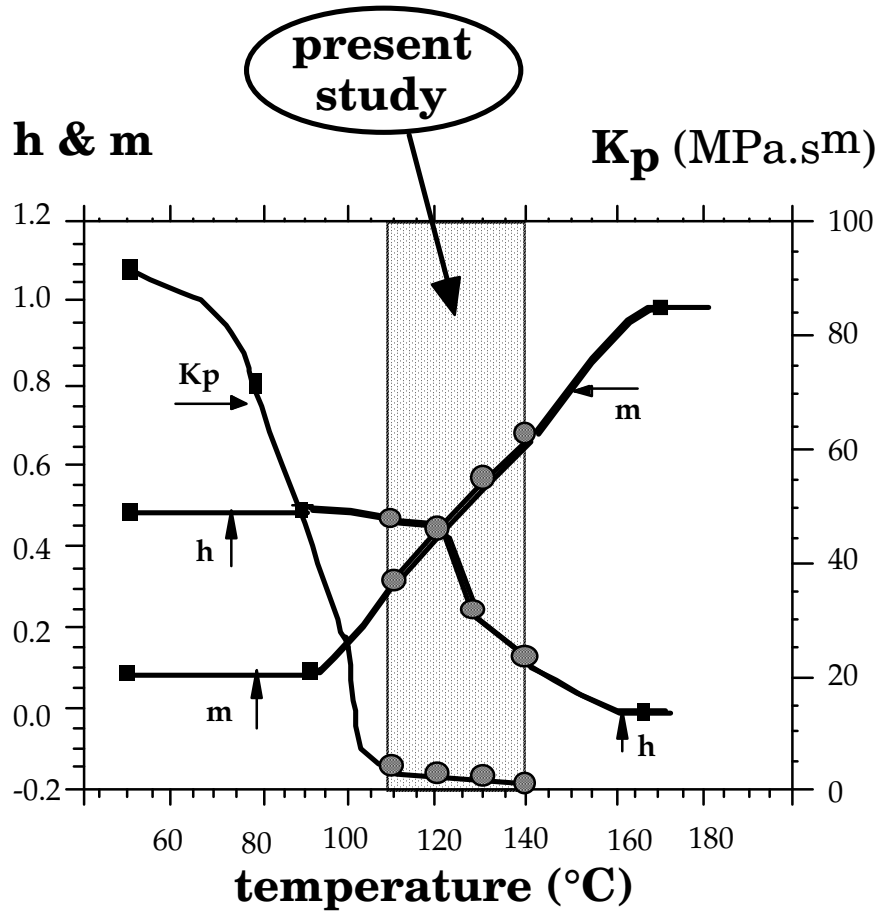

Figure 5 : Thermal dependence of rheological coefficients m, h and K_p(MPa.s^m). Black squares issued from [10]).

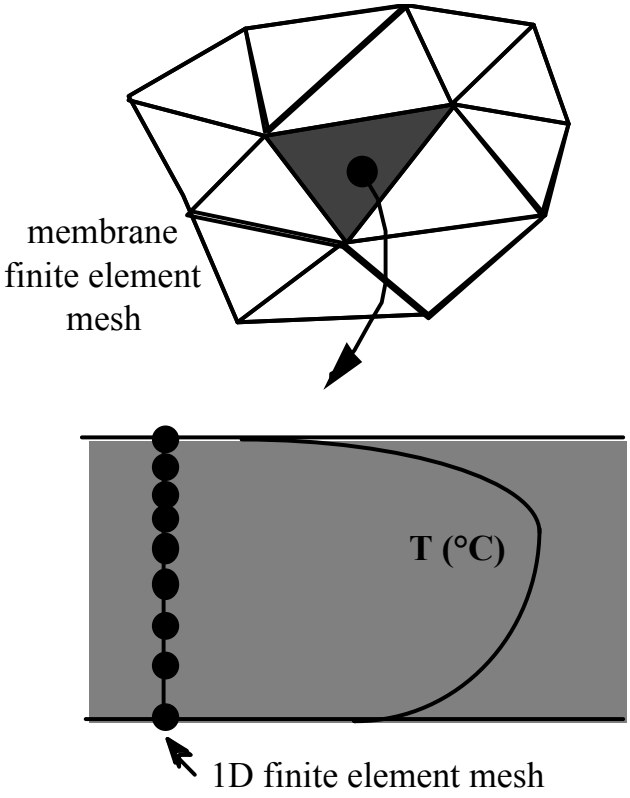

Figure 6 : One-dimensional approach through the sheet thickness for thermal coupling.

A/ Thermal resolution

- for all membrane elements
  - for all integration points of the element
    - perform a 1D finite element computation of the new temperature profile T' across the thickness. The source term is given by the mechanical resolution of previous time step.
    - for all integration points "ip_th" of the 1D mesh

    update the temperature-dependent coefficients: $K'_p(T')$, m'(T') and h'(T').

B/ Mechanical resolution

B1) computation of the residual vector $\mathbf{R}(\mathbf{U})$

- for all membrane elements
  - for all integration points of the element
    - for all integration points "ip_th" of the 1D mesh

      solve the constitutive equations for $\boldsymbol{\sigma}'$(ip_th) and $\partial\boldsymbol{\sigma}'/\partial\Delta\boldsymbol{\varepsilon}$(ip_th), using the updated values of material coefficients: K'_p(ip_th), m'(ip_th) and h'(ip_th)
    - compute thickness-averaged values $\langle\boldsymbol{\sigma}'\rangle$ and $\langle\partial\boldsymbol{\sigma}'/\partial\Delta\boldsymbol{\varepsilon}\rangle$ and sum in residual vector.

B2) iterative Newton-Raphson procedure to solve $\mathbf{R}(\mathbf{U})=\mathbf{0}$

Figure 7 : Thermo-mechanical coupling algorithm.

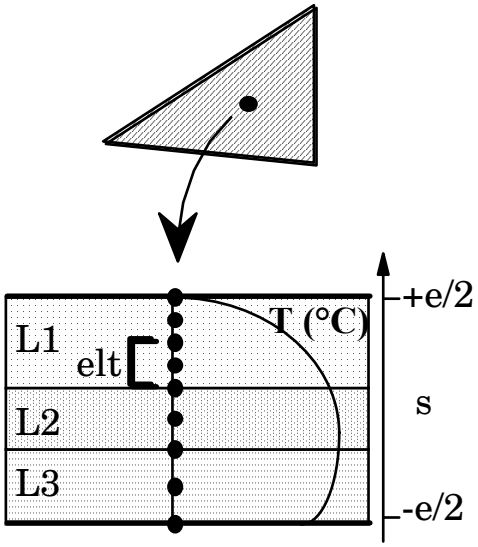

Figure 8 : Multi-layer approach with thermal and rheological gradients (here in the case of three layers, using four quadratic one-dimensional finite elements through the thickness).

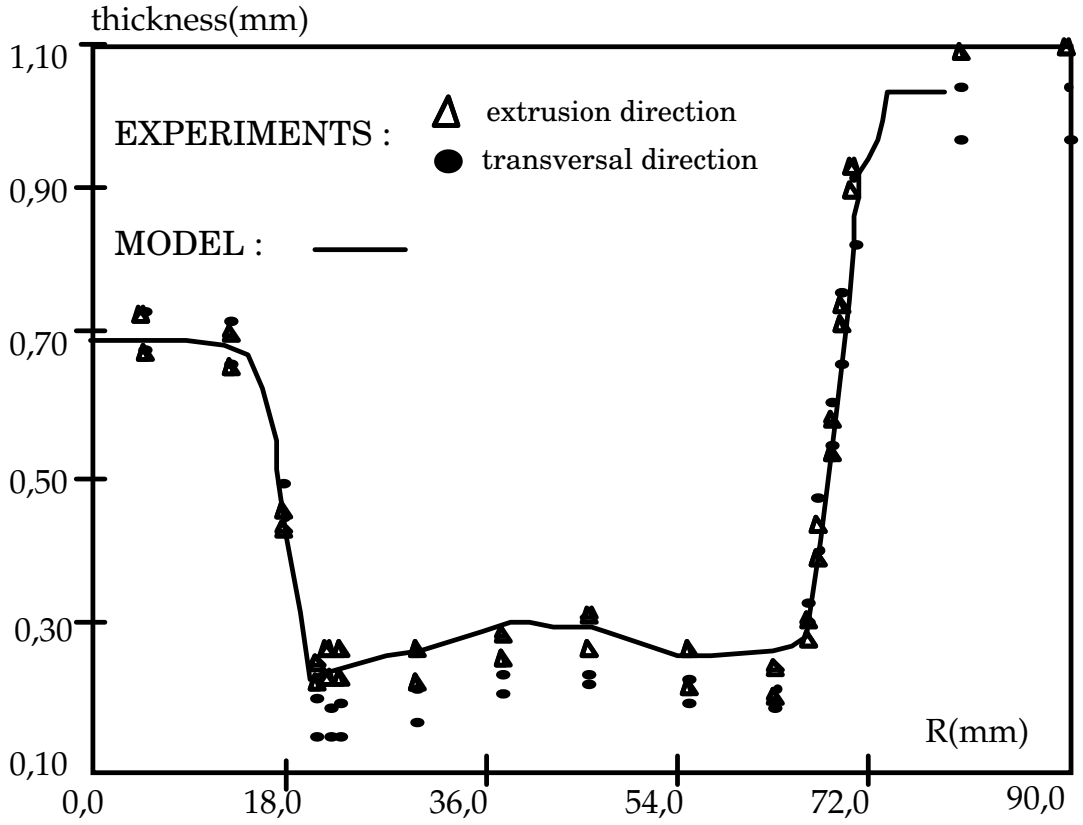

Figure 9 : Comparison between computed (solid line) and measured thickness distribution along the extrusion and transverse directions after an axisymmetrical forming with a central insert.

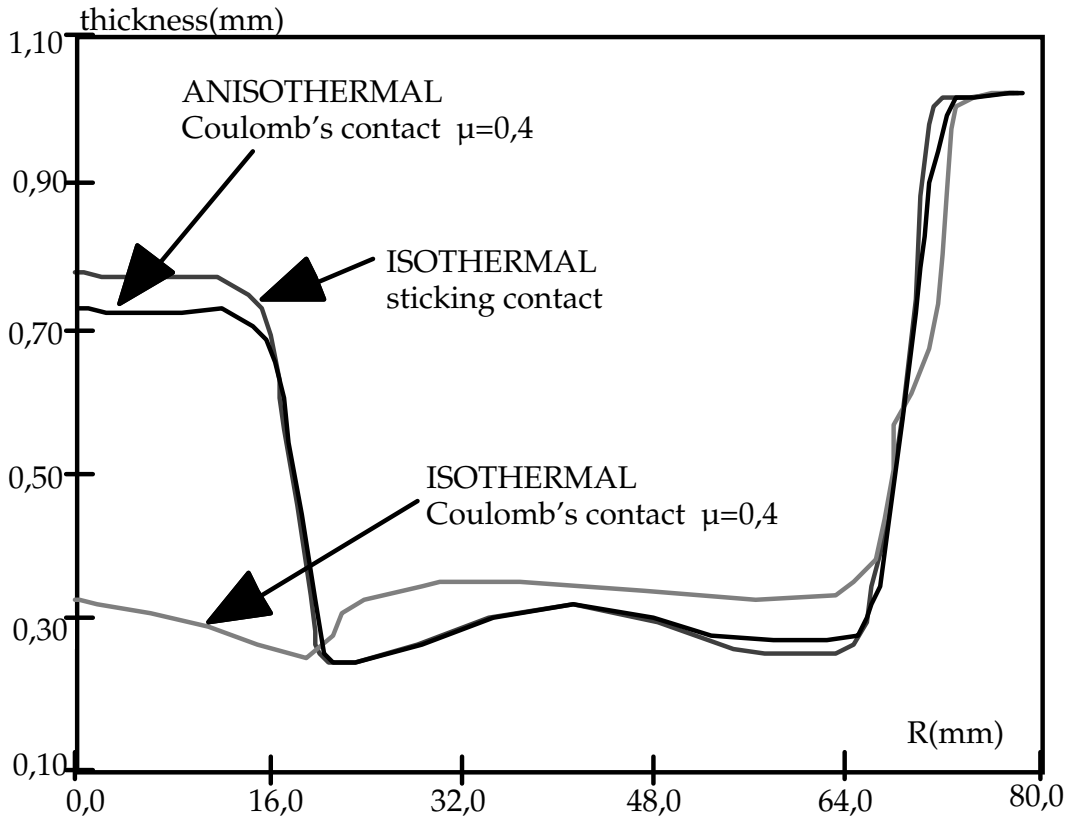

Figure 12 : Computed thickness profile showing the respective influence of thermal coupling and contact conditions.

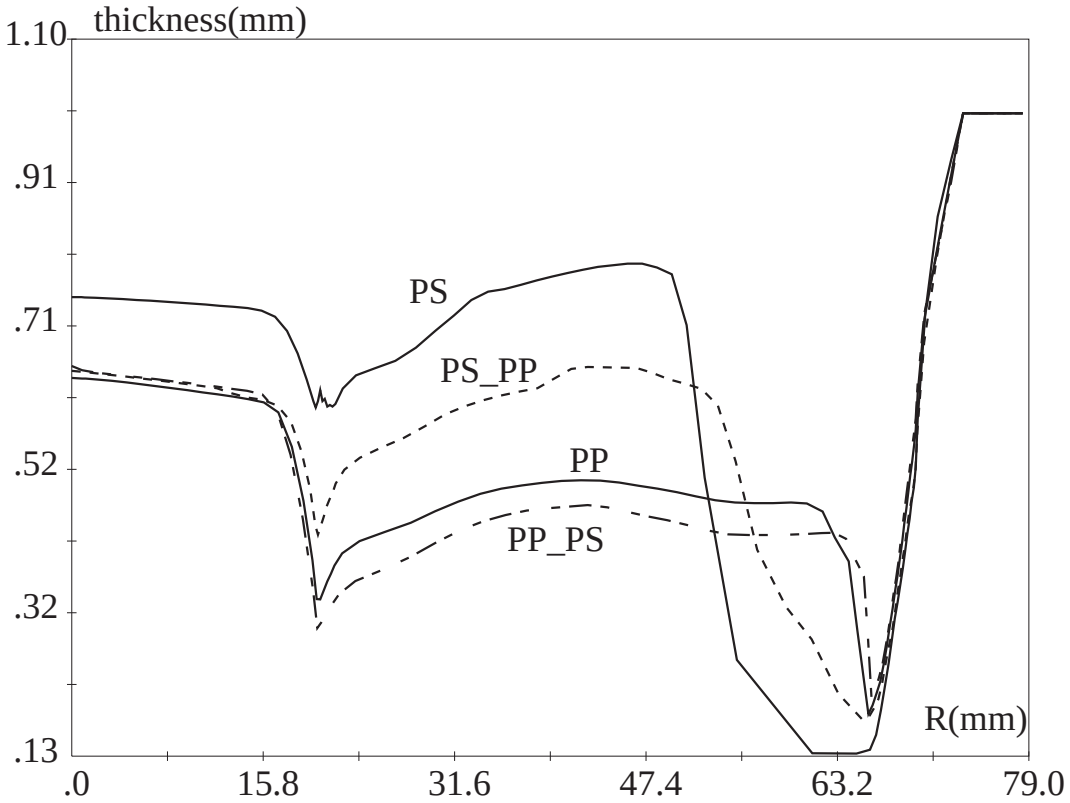

Figure 16 : Computed thickness profile of bi-layered films (polypropylene or polystyrene on top) formed with a punch compared with the pure polymers: Temperature = 150 °C; Pressure rate = 1.6 MPa/s.

PP only	PP_PS PP on top	PS_PP PS on top	PS only
0.59 s	0.50 s	0.39 s	0.45 s

Table 1 - Prediction of forming time for the bilayer and pure films (see processing conditions in the text).

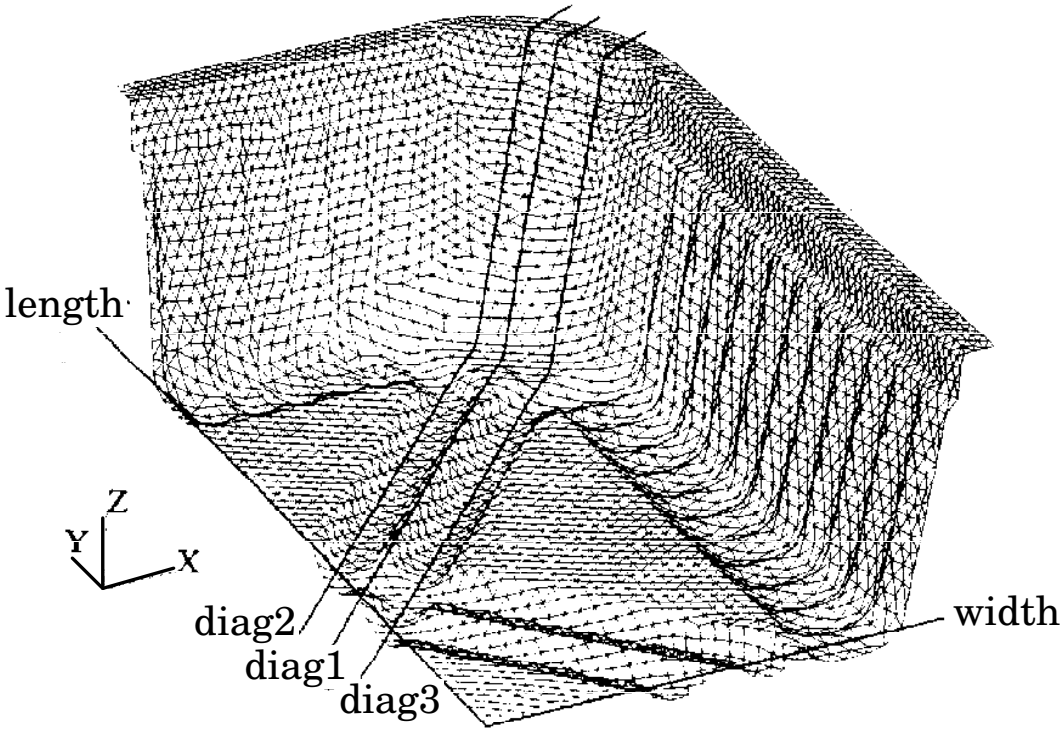

Figure 19 : Final deformed finite element mesh and selected directions for the thickness comparison.

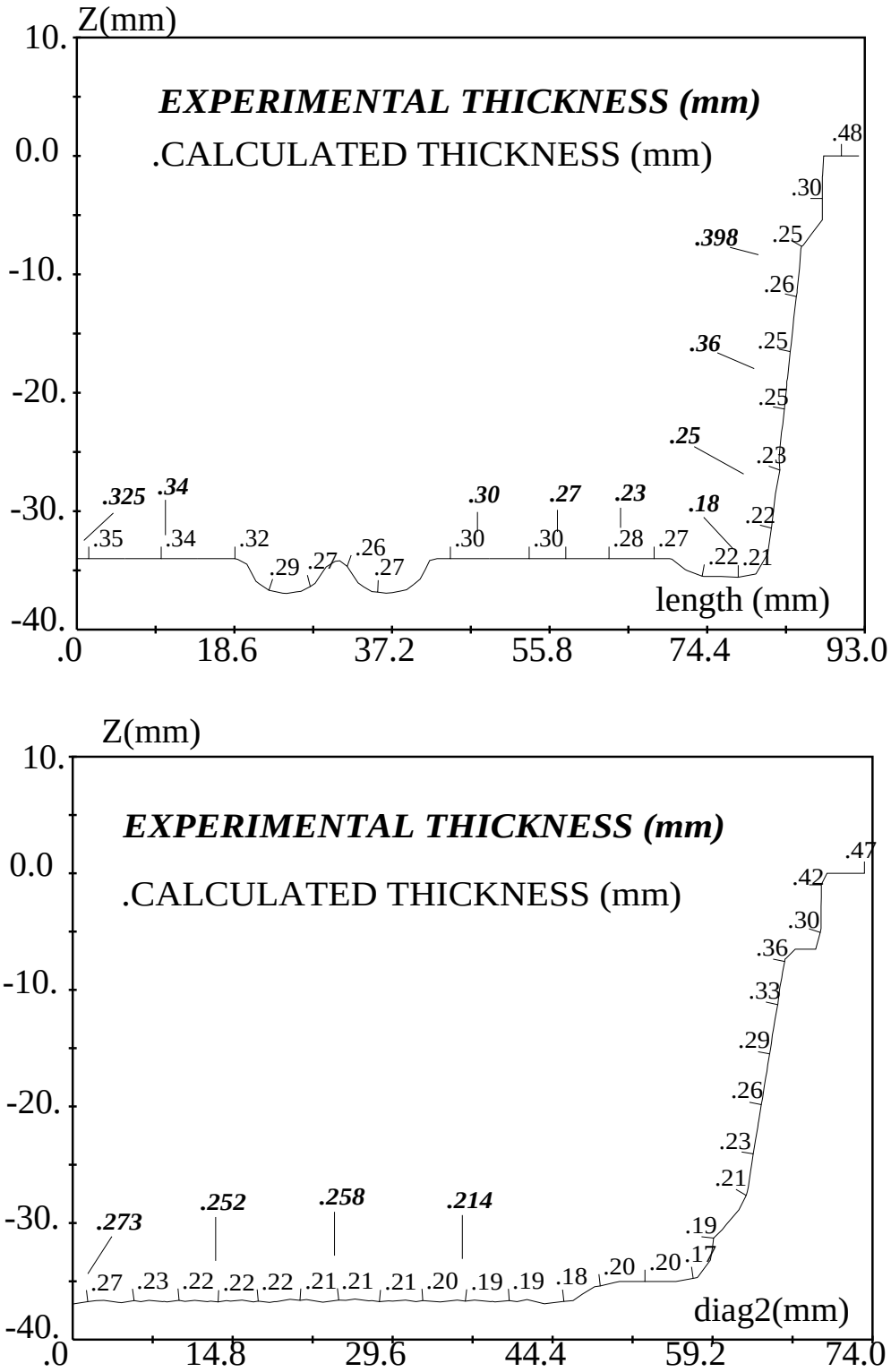

Figure 20 : Example of comparison of measured and computed thickness a: "length" and b: "diag2" directions on figure 19).